



| | |
|--------------|--|
| Title | Peak Power Properties of Band-Limited Signals: With Pulse Shaping Or Windowing |
| Author(s) | Ochiai, Hideki |
| Citation | IEEE Transactions on Vehicular Technology. 2024, 73(10), p. 15200-15213 |
| Version Type | VoR |
| URL | https://hdl.handle.net/11094/97850 |
| rights | This article is licensed under a Creative Commons Attribution 4.0 International License. |
| Note | |

The University of Osaka Institutional Knowledge Archive : OUKA

<https://ir.library.osaka-u.ac.jp/>

The University of Osaka

Peak Power Properties of Band-Limited Signals: With Pulse Shaping Or Windowing

Hideki Ochiai, *Fellow, IEEE*

Abstract—The signal with high spectral efficiency tends to suffer from high peak-to-average power ratio (PAPR), which significantly reduces the achievable power amplifier efficiency. Therefore, it is important to investigate the statistical properties of *band-limited* signals in terms of their dynamic range. On the other hand, the out-of-band (OOB) emission of signals can be controlled by pulse shaping or windowing, where the latter is generally applicable to block transmission systems such as orthogonal frequency-division multiplexing (OFDM). In this work, by developing closed-form expressions of high-order moments for the signals band-limited by the conventional raised-cosine (RC) as well as square-root raised-cosine (RRC) filtering, we discuss the trade-off relationship between the spectral efficiency and signal dynamic range. In addition, an expression for the complementary cumulative distribution function (CCDF) of the instantaneous power in the case of *filtered* Gaussian signals is developed. Based on these theoretical analyses, we elucidate the fact that as the transmit symbols approach Gaussian for increasing spectral efficiency, the resulting *filtered* signals tend to exhibit even higher dynamic range compared to the conventional block transmission systems such as OFDM and DFT-precoded OFDM.

Index Terms—High-order moment, orthogonal frequency-division multiplexing (OFDM), peak-to-average power ratio (PAPR), single-carrier signal, (square-root) raised-cosine filter.

I. INTRODUCTION

Future wireless communications such as the sixth generation (6G) cellular networks should support ultra high spectral efficiency with ultra low power consumption. In order to realize such a system, it is important to take into account the power amplifier efficiency of the transmitter, which depends on the dynamic range of transmit signals [1]. This naturally motivates a fundamental study on the design of band-limited signals with high spectral efficiency *and* low peak power.

Many existing high-speed communications standards adopt orthogonal frequency division multiplexing (OFDM)-based systems, where multiple symbols are merged into one block (i.e., OFDM symbol) through inverse discrete Fourier transform (IDFT) and transmitted simultaneously. The major drawback of OFDM systems over the conventional single-carrier systems is their signal with high peak-to-average power ratio (PAPR) [2], since the OFDM signal is characterized by a band-limited complex Gaussian random process that has unbounded signal dynamic range in principle.

To cope with this issue, DFT-precoded (or DFT-spread) OFDM has been adopted by the fourth generation (4G), which is also known as single-carrier frequency-division multiple access (SC-FDMA) as it is essentially a block transmission of single-carrier signals based on *sinc*-like periodic pulse shaping filter generated by oversampling [3].

These block transmission systems can cope with frequency-selective channels by the use of cyclic prefix (CP), which makes complex time-domain equalization unnecessary. The price is its overhead of introducing CP, which may lead to reduction of spectral efficiency.

Several variations of OFDM have been proposed, such as generalized frequency division multiplexing (GFDM) [4] and orthogonal time frequency space (OTFS) modulation [5]. As a result, the PAPR properties of these signals have received significant attention. In [6], the PAPR properties of GFDM have been analyzed, whereas those of OTFS modulated signal have been studied in [7, 8].

In practice, the transmit signal should be band-limited by reducing out-of-band (OOB) emission. To this end, one can employ the conventional pulse shaping, or windowing in the case of block transmission [9, 10]. As a result, the above-mentioned works [6–8] investigate the effect of the conventional pulse shaping filters such as raised-cosine (RC) filter with a specific roll-off factor (i.e., the excess bandwidth parameter) α . It is important to note that for the system with RC or square-root raised-cosine (RRC) filters, its roll-off factor not only determines the spectral efficiency of the system, but also affects its signal dynamic range [11]. In general, there is a trade-off relationship between the spectral efficiency and dynamic range of the resulting signal as well as its cost for implementation. Specifically, reducing α leads to higher spectral efficiency, but it causes severe signal envelope fluctuation as well as increases the effective impulse response span, which renders its practical implementation more challenging.

Based on the above observation, this work focuses on the statistical behavior of single-carrier signals pulse-shaped by the RC and RRC filters as they are most commonly adopted benchmarks in the conventional communications systems with linear modulation. In order to fully characterize their signal dynamic range, the statistical distributions of the instantaneous power of band-limited signals, often in the form of the complementary cumulative distribution function (CCDF), should be examined. However, their evaluation process usually involves numerical integration that requires some computational effort or Monte-Carlo methods, rendering further theoretical analysis infeasible. Therefore, as a tractable tool for statistical analysis, the high-order moment expressions of linearly modulated signals [12] will be adopted in this work. Unlike CCDF,

© 2024 IEEE. Personal use of this material is permitted. However, permission to use this material for any other purposes must be obtained from the IEEE by sending a request to pubs-permissions@ieee.org. The author is with Graduate School of Engineering, Osaka University, 2-1 Yamadaoka, Suita, Osaka 565-0871, Japan. This work was supported in part by the Japan Society for the Promotion of Science (JSPS) through the Grants-in-Aid for Scientific Research (KAKENHI) under Grant 21H04873. (email: ochiai@comm.eng.osaka-u.ac.jp)

the high-order moments are single numerical metrics that are easy to evaluate and compare. Moreover, they can often be expressed in closed forms.

In [6, 8], it has been identified that the use of RC filtering for GFDM and OTFS systems will lead to higher PAPR due to the non-stationarity of the resulting signals compared to the conventional system without RC filtering. Nevertheless, the dependence of pulse shaping filters and their roll-off factors (i.e., spectral efficiency) on the signal dynamic range has not been fully explored. We also note that the previous study in [12] was limited to the case with $\alpha = 0$, i.e., the pulse shaping filter characterized by the ideal sinc function, practically implementable by block transmission with windowing.

According to the information theory, the optimal modulation over an additive white Gaussian noise (AWGN) channel under average power constraint is Gaussian. Moreover, the application of constellation shaping with optimal coding will shift the achievable performance of practical finite constellation systems toward Shannon limit, but in return the transmit signal should approach complex Gaussian distribution. In addition, not only the conventional OFDM, but also other modern communication systems such as GFDM, OTFS modulation, and even non-orthogonal multiple access (NOMA) [13, 14], make their time-domain signal samples approach Gaussian due to the central limit theorem, since several independent signal components are linearly combined to form each transmit symbol, possibly through some precoding or spreading processes. Therefore, it is of both theoretical and practical interest to investigate single-carrier systems where Gaussian distributed modulation is applied.

In this work, we will show that the optimal roll-off factor from the viewpoint of signal dynamic range depends on the modulation formats, and also explicitly demonstrate that when the signal samples approach Gaussian, pulse shaping that does not maintain signal stationarity should not be employed. In such a case, they should be combined with rectangular pulse, letting smooth windowing [9, 10] take care of the OOB emission as a practical low-complexity countermeasure.

The main contributions of this work are summarized as follows:

- We derive the fourth and sixth-order moments of conventional single-carrier signals band-limited by the RC and RRC filters of an arbitrary roll-off factor α . It will be shown that the results are given in closed-form expressions that can readily be evaluated without any numerical integration.
- Based on the developed expressions, we describe how the dynamic range of the RC and RRC-filtered signals will be affected by the roll-off factor α from the viewpoint of the fourth and sixth order moments. Interestingly, reducing α does not always increase the signal dynamic range.
- In order to investigate how dynamic range will be affected by Gaussianity of transmit symbols, the fourth and sixth-order moments of clipped Gaussian signals (as an example of quasi-Gaussian signals) are also analyzed with RC and RRC filtering.
- We prove that the case with $\alpha = 0$ (i.e., ideal rectangular filter with no excess bandwidth) is in fact optimal for

Gaussian signal, as was previously observed in [15]. To this end, the CCDF expression of the instantaneous power for the *filtered* Gaussian signals is also developed.

- Based on the above-mentioned theoretical results, we conclude that as long as the symbol to be transmitted is close to Gaussian, the conventional block transmission (with sinc-like pulse shaping) should be preferable from the viewpoint of signal dynamic range.

This paper is organized as follows. Section II introduces notations and signal models, as well as reviews their statistical measures such as CCDF of instantaneous power and its connection to high-order moments. Section III describes the properties of RC and RRC filters and analyzes the energy loss due to truncation of their impulse responses. The CCDF properties of single-carrier signals pulse-shaped by RC and RRC filters are also discussed, showing that $\alpha = 0$ is optimal when the transmit symbol follows Gaussian. In Section IV, we review the expressions of the high-order moments of linearly modulated signals based on a linear combination of cumulants, and then introduce clipped Gaussian signal model as an example of quasi-Gaussian distribution. We then show numerical examples of the fourth and sixth-order moments for these signals with RC and RRC filtering in Section V. Finally, Section VI concludes this work. Some of the results on the fourth-order moment in this paper were initially reported in [16] without rigorous proofs.

II. SIGNAL MODELS AND THEIR HIGH-ORDER MOMENTS

We start with a general description of complex baseband signals that are subject to restriction in terms of their bandwidth. The motivation for investigating their fourth and sixth-order moments is reviewed first.

A. Moments of Band-Limited Signals

We use $s(\tau)$ to denote a complex baseband signal where the time-scale is normalized by the Nyquist rate, i.e., at which one complex-valued symbol such as quadrature amplitude modulation (QAM) is transmitted. In other words, one QAM symbol is transmitted per the time interval $[0, 1)$. Since our interest is on the dynamic range of band-limited signals to be transmitted, we will focus on the distribution of their instantaneous power. A widely accepted metric is the CCDF of the instantaneous power $p(\tau) \triangleq |s(\tau)|^2$ for a given time instant τ , which is given by

$$\text{CCDF}(\zeta | \tau) \triangleq \Pr [p(\tau) \geq \zeta], \quad (1)$$

where ζ corresponds to the threshold value (reference level) of instantaneous power. When the instantaneous power of the signal is stationary in a strict sense, one can select an arbitrary time instant τ from $[0, 1)$ to characterize its distribution. On the other hand, if the signal is cyclo-stationary over the symbol period $[0, 1)$, then the following time-averaged CCDF should be of interest:

$$\text{CCDF}(\zeta)_{\text{av}} \triangleq \int_0^1 \text{CCDF}(\zeta | \tau) d\tau. \quad (2)$$

By Markov inequality, for any positive integer n , we have

$$\text{CCDF}(\zeta | \tau) \leq \frac{1}{\zeta^n} E \{ p^n(\tau) \} = \frac{1}{\zeta^n} \underbrace{E \{ |s(\tau)|^{2n} \}}_{\triangleq m_{2n}(s(\tau))}, \quad (3)$$

for any $\zeta > 0$, where $E\{\cdot\}$ denotes an expectation operation, and thus $m_{2n}(s(\tau))$ corresponds to the $2n$ th-order moment of the complex signal envelope $|s(\tau)|$. Therefore, for a given reference level ζ , if the n th moments of $p(\tau)$ are smaller for $n \geq 2$, then we may expect that the corresponding CCDF value is lower, even though the above upper bound may not be tight in general. Taking the time average of (3) over the interval $[0, 1)$, we may write

$$\text{CCDF}(\zeta)_{\text{av}} \leq \frac{1}{\zeta^n} \overline{m_{2n}}, \quad (4)$$

where

$$\overline{m_{2n}} \triangleq \int_0^1 m_{2n}(s(\tau)) d\tau \quad (5)$$

is the time-averaged $2n$ th-order moment of $|s(\tau)|$.

We are particularly interested in the above moments with $n = 2$ and $n = 3$, i.e., the fourth and sixth-order moments of the signal along with time averaging. The former corresponds to a *power variance* [17, 18], whereas the latter is equivalent to the cubic metric [19–21], both of which are considered as alternative metrics for signal dynamic range that are more tractable than the conventional distributions of PAPR or instantaneous power. The primary advantage of studying the high-order moments is that they can often be expressed in closed forms. In [22], the high-order moments of PAPR for complex Gaussian signals are derived.

B. Pulse Shaping System

A pulse shaped baseband signal can be expressed as

$$s_{\text{P}}(t) = \sum_{k=-\infty}^{\infty} X_k g_{\text{P}}(t - kT), \quad (6)$$

where $g_{\text{P}}(t)$ is the impulse response of a given pulse shaping filter with T corresponding to the Nyquist rate, $X_k \in \mathcal{X}$ is the k th modulated symbol, and \mathcal{X} is a set of constellation points, typically chosen from a family of QAM.

Without loss of generality, we normalize the time scale by the Nyquist rate (in accordance with the model introduced in the previous subsection) and redefine $g(\tau) \triangleq g_{\text{P}}(\tau T)$ as the normalized impulse response. We then rewrite the signal (6) with $s(\tau) \triangleq s_{\text{P}}(\tau T)$ as

$$s(\tau) = \sum_{k=-\infty}^{\infty} X_k g(\tau - k). \quad (7)$$

Assuming that $\{X_k\}$ are independent and identically distributed (i.i.d.) with zero mean and unit variance, the second

moment of the signal defined in (3) with $n = 1$ is expressed as

$$\begin{aligned} m_2(s(\tau)) &= E \{ |s(\tau)|^2 \} \\ &= \sum_{k=-\infty}^{\infty} E \{ |X_k|^2 \} |g(\tau - k)|^2 \\ &= \sum_{k=-\infty}^{\infty} |g(\tau - k)|^2. \end{aligned} \quad (8)$$

Since k is an integer, it follows that the second moment is cyclo-stationary over $[0, 1)$ in general. In practice, the time interval of $s(\tau)$ should be finite, and thus the impulse response of pulse shaping filter must be truncated with sufficient interval and smoothly enough to avoid excessive OOB. The amount of energy loss due to the truncation will be discussed in Section III in the cases of RC and RRC filters.

C. Block Transmission System

We next define the block transmission signal as

$$s_{\text{B}}(t) = \sum_{\ell=-\infty}^{\infty} g_{\text{w}}(t - \ell T_s) s_{\ell}(t - \ell T_s), \quad (9)$$

where $g_{\text{w}}(t)$ is a windowing function that controls the sidelobe of power spectrum of transmit signals, T_s is a block length of the signal including cyclic prefix and postfix, and $s_{\ell}(t)$ is the ℓ th block with ℓ representing the block index. Let $T_s = T_{\text{ex}} + T_u$, where T_{ex} is the length of extra part (cyclic prefix and postfix) and $T_u = NT$ is the effective (useful) period of each block, with T corresponding to the Nyquist rate. The effect of windowing on the spectral efficiency of OFDM systems is discussed in [10]. Since windowing does not affect the peak power property [23], we can focus only on a single baseband block $s_{\ell}(t)$ with $t \in [0, T_u)$.

1) *OFDM*: In the case of OFDM, the ℓ th baseband symbol with N subcarriers can be expressed as

$$s_{\ell}(t) = \frac{1}{\sqrt{N}} \sum_{n=0}^{N-1} X_{\ell,n} e^{j2\pi(n - \frac{N-1}{2}) \frac{t}{T_u}}, \quad (10)$$

where $X_{\ell,n} \in \mathcal{X}$ is a transmit symbol on the n th subcarrier of the ℓ th block (i.e., OFDM symbol).

We normalize the time scale of $s_{\ell}(t)$ as $\tau = t/T$, where $T = T_u/N$, and redefine the OFDM symbol, hereafter dropping the OFDM symbol index ℓ for simplicity, as

$$\begin{aligned} s(\tau) &= \frac{1}{\sqrt{N}} \sum_{n=0}^{N-1} X_n e^{j2\pi(n - \frac{N-1}{2}) \frac{\tau}{N}} \\ &= \sum_{n=0}^{N-1} X_n \hat{g}_n(\tau), \quad 0 \leq \tau < N, \end{aligned} \quad (11)$$

where

$$\hat{g}_n(\tau) \triangleq \frac{e^{j\varphi\tau}}{\sqrt{N}} e^{j2\pi \frac{n}{N} \tau}, \quad \varphi \triangleq \frac{1-N}{N} \pi \quad (12)$$

can be seen as an impulse response for the n th subcarrier, which is simply a complex sinusoid with distinct frequency.

The impulse responses $\{\hat{g}_n(\tau)\}$ are orthogonal over the time interval $[0, N)$, i.e.,

$$\int_0^N \hat{g}_n(\tau) \hat{g}_m^*(\tau) d\tau = \delta_{n,m}, \quad (13)$$

where $\delta_{n,m}$ is the Kronecker delta with $\delta_{n,m} = 1$ if $n = m$ and $\delta_{n,m} = 0$ otherwise.

Assuming that $\{X_n\}$ are all zero-mean and unit-variance (standardized) random variables, as well as i.i.d., the second moment of the signal (11) is given by

$$m_2(s(\tau)) = \sum_{n=0}^{N-1} |\hat{g}_n(\tau)|^2 E\{|X_n|^2\} = 1. \quad (14)$$

Therefore, the second moment of the OFDM symbol is stationary over the symbol period $[0, N)$. We note that the fourth and sixth-order moments of $s(\tau)$ are also stationary (i.e., they do not depend on τ) over $[0, N)$ as long as \mathcal{X} is chosen from the standard QAM constellations (see Theorems 11 and 13 of [12]).

2) *DFT-Precoded OFDM*: In the case of DFT-precoded OFDM, let X_n in (11) be replaced by

$$\tilde{X}_n = \frac{1}{\sqrt{N}} \sum_{k=0}^{N-1} X_k e^{-j2\pi \frac{k}{N} n}, \quad (15)$$

where $X_k \in \mathcal{X}$ corresponds to the k th QAM symbol in the time domain (i.e., the modulated symbol prior to DFT precoding). Substitution of \tilde{X}_n in (15) into X_n of (11) yields

$$s(\tau) = \sum_{k=0}^{N-1} X_k \underbrace{\frac{1}{N} e^{j\varphi\tau} \sum_{n=0}^{N-1} e^{j2\pi \frac{n}{N} (\tau-k)}}_{\triangleq \tilde{g}_k(\tau)}, \quad (16)$$

where $\tilde{g}_k(\tau)$ corresponds to a complex impulse response applied to QAM symbols $\{X_k\}$. With some algebra, we may rewrite (16) as [3]

$$s(\tau) = \sum_{k=0}^{N-1} X_k \underbrace{e^{-jk(1-\frac{1}{N})\pi} \frac{\sin(\pi(\tau-k))}{N \sin(\frac{\pi}{N}(\tau-k))}}_{\triangleq \tilde{g}_k(\tau)}, \quad (17)$$

where the impulse response $\tilde{g}_k(\tau)$ of (16) can now be regarded as a periodic sinc function (Dirichlet kernel).

From (16), we notice that

$$\begin{aligned} \sum_{k=0}^{N-1} |\tilde{g}_k(\tau)|^2 &= \frac{1}{N^2} \sum_{n=0}^{N-1} \sum_{\ell=0}^{N-1} e^{j2\pi \frac{n-\ell}{N} \tau} \underbrace{\sum_{k=0}^{N-1} e^{-j2\pi \frac{(n-\ell)k}{N}}}_{N \delta_{n,\ell}} \\ &= \frac{1}{N} \sum_{n=0}^{N-1} \sum_{\ell=0}^{N-1} e^{j2\pi \frac{n-\ell}{N} \tau} \delta_{n,\ell} = 1. \end{aligned} \quad (18)$$

It thus follows from (17) that

$$\sum_{k=0}^{N-1} \left| \frac{\sin(\pi(\tau-k))}{N \sin(\frac{\pi}{N}(\tau-k))} \right|^2 = 1 \quad (19)$$

for any τ . In other words, similar to OFDM, we have

$$E\{|s(\tau)|^2\} = \sum_{k=0}^{N-1} |\tilde{g}_k(\tau)|^2 E\{|X_k|^2\} = 1 \quad (20)$$

and thus the second moment is stationary for DFT-precoded OFDM as long as $\{X_k\}$ are chosen as i.i.d. random variables. Nevertheless, unlike OFDM, the fourth (and higher) order moments may not be stationary. Therefore, the distribution of their instantaneous power depends on τ .

3) *PAPR and Instantaneous Power*: In the case of block transmission, the signal dynamic is often characterized by the peak-to-average power ratio (PAPR) of the signal defined as

$$\text{PAPR} = \max_{0 \leq \tau < N} |s(\tau)|^2, \quad (21)$$

which should grow with N , as observed in [2] for the case of Gaussian signals. A more relevant measure in terms of power amplifier efficiency is the distribution of the time-averaged instantaneous power as defined in (2). In the case of OFDM, as $N \rightarrow \infty$, $s(\tau)$ approaches Gaussian due to the central limit theorem for each τ . Furthermore, $s(\tau)$ has a unit variance and thus should be stationary. The CCDF of the instantaneous power is then expressed for any τ as

$$\text{CCDF}(\zeta | \tau) = e^{-\zeta}. \quad (22)$$

On the other hand, CCDF may vary depending on τ in the case of DFT-precoded OFDM unless $\{X_k\}$ are Gaussian distributed, since the weights of symbols $\{X_k\}$ that form a linearly combined signal may vary depending on τ [24, 25]. The CCDF property will be investigated numerically in the next section.

III. RC AND RRC FILTERS

Theoretical analysis and practical implementation of pulse shaping filters that satisfy Nyquist's first criterion, commonly referred to as Nyquist filters, have been an important area of research that targets realization of strictly band-limited communication systems. Among many possible descriptions of Nyquist filters, the raised-cosine (RC) filter is a common benchmark mainly due to its simple frequency response expression from a mathematical viewpoint. Several Nyquist (or quasi-Nyquist) filters have been proposed that are better than the conventional RC filter from a practical viewpoint such as robustness against timing jitters or reduction of inter-symbol interference (ISI) [26–28].

In practical single-carrier systems, the matched filtering modification of the RC filter, i.e., the square-root raised-cosine (RRC) filter, has been adopted so as to maximize the signal-to-noise power ratio (SNR) at the receiver [29]. Similar to RC filtering, the primary advantage of RRC filtering may be its feasibility in terms of mathematical description as well as its implementation. It has thus served as a common benchmark for the square-root Nyquist filter family, and related recent studies include filtering design suitable for the faster than Nyquist signaling [30] and machine learning based waveform design [31], where the RRC filter is adopted as their benchmark.

In this section, we review these filters as well as the properties of the resulting signals.

A. Frequency Response

Without loss of generality, we consider the case where the Nyquist interval is normalized to unity for simplicity of notation, following the signal model introduced in the previous section. In general, the frequency response of Nyquist filters (including their square-root forms) can be expressed by a real and even function as

$$G(f) = \begin{cases} K, & 0 \leq |f| \leq \frac{1-\alpha}{2}, \\ K G_{\text{tr}}(f), & \frac{1-\alpha}{2} < |f| \leq \frac{1+\alpha}{2}, \\ 0, & |f| > \frac{1+\alpha}{2}, \end{cases} \quad (23)$$

where $\alpha \in [0, 1]$ is the roll-off factor (or excess bandwidth parameter) that determines the bandwidth of the transmit signals, K is a positive constant for energy normalization, and $G_{\text{tr}}(f)$ is a transition function that adjusts the spectrum shape. Note that $\alpha = 0$ corresponds to the ideal low-pass filter. Reducing α thus enhances the spectral efficiency but at the cost of increasing signal dynamic range (i.e., loss in terms of peak power efficiency) as well as increasing complexity for practical implementation associated with the effective (non-negligible) length of impulse response.

In the cases of RC and RRC filters, we may express

$$G_{\text{tr}}(f) = \begin{cases} \cos^2 \left[\frac{\pi}{2\alpha} \left(|f| - \frac{1-\alpha}{2} \right) \right], & \text{RC}, \\ \cos \left[\frac{\pi}{2\alpha} \left(|f| - \frac{1-\alpha}{2} \right) \right], & \text{RRC}. \end{cases} \quad (24)$$

The constant K is chosen to meet the energy constraint

$$\int_{-\infty}^{\infty} G^2(f) df = 1, \quad (25)$$

and thus we have

$$K = \begin{cases} \sqrt{\frac{4}{4-\alpha}}, & \text{RC}, \\ 1, & \text{RRC}. \end{cases} \quad (26)$$

B. Impulse Response

The impulse response $g(\tau)$ of a given filter can be obtained by directly applying the inverse Fourier transform to $G(f)$. Since $G(f)$ is real and even, we have

$$g(\tau) = 2 \int_0^{\infty} G(f) \cos(2\pi f) df. \quad (27)$$

Substitution of (23) with (24) into (27) yields

$$g(\tau) = \begin{cases} \sqrt{\frac{4}{4-\alpha}} \text{sinc}(\pi\tau) \frac{\cos(\pi\alpha\tau)}{1-(2\alpha\tau)^2}, & \text{RC}, \\ \frac{\sin(\pi(1-\alpha)\tau) + 4\alpha\tau \cos(\pi(1+\alpha)\tau)}{\pi\tau\{1-(4\alpha\tau)^2\}}, & \text{RRC}, \end{cases} \quad (28)$$

where $\text{sinc}(x) \triangleq \sin(x)/x$. Note that if the denominator in (28) becomes zero, it should be replaced by the corresponding limit using L'Hôpital's rule [32].

By Parseval's Theorem and (25), we have

$$\int_{-\infty}^{\infty} g^2(\tau) d\tau = \int_{-\infty}^{\infty} G^2(f) df = 1, \quad (29)$$

indicating that the energy of the impulse responses (28) is also normalized.

In Fig. 1, the impulse responses $g(\tau)$ are plotted for $\alpha = 0$ (sinc function), 0.5, and 1.0. We observe that in the case of low roll-off factor, the impulse response diminishes only slowly, whereas it converges to zero quickly as α increases.

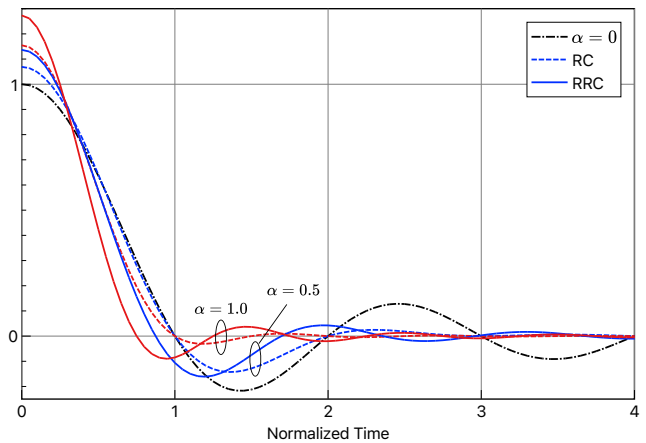


Fig. 1. Impulse responses of RC and RRC filters with roll-off factors of $\alpha = 0$ (sinc function), 0.5, and 1.0.

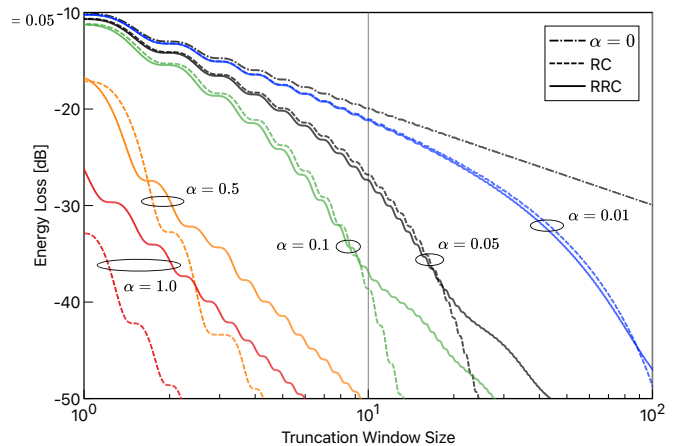


Fig. 2. The relationship between the window size (τ_0) and energy loss $L(\tau_0)$ for the RC and RRC filters with several different roll-off factors.

C. Second Moment of Filtered Signal

From (8) and Appendix A, the second moment of the filtered signal according to $G(f)$ of (23) can be simplified as

$$m_2(s(\tau)) = 1 + b_2 \cos(2\pi\tau), \quad (30)$$

where b_2 is a constant that can be calculated by (A-8) shown in Appendix A, and $b_2 = 0$ if and only if $G(f)$ has an ideal rectangular shape (i.e., $\alpha = 0$). As a result, unless $\alpha = 0$, the second moment of Nyquist-filtered signals is cyclo-stationary with unit period.

Note that in the cases of RC and RRC filters, b_2 is given by

$$b_2 = \begin{cases} \frac{\alpha}{4-\alpha}, & \text{RC}, \\ \frac{2\alpha}{\pi}, & \text{RRC}, \end{cases} \quad (31)$$

as discussed in Appendix B.

D. Energy Loss Due to Truncation

If a pulse shaping filter of infinite support is to be applied to block transmission system, it is necessary to truncate the impulse response and make them periodic. Here, one major

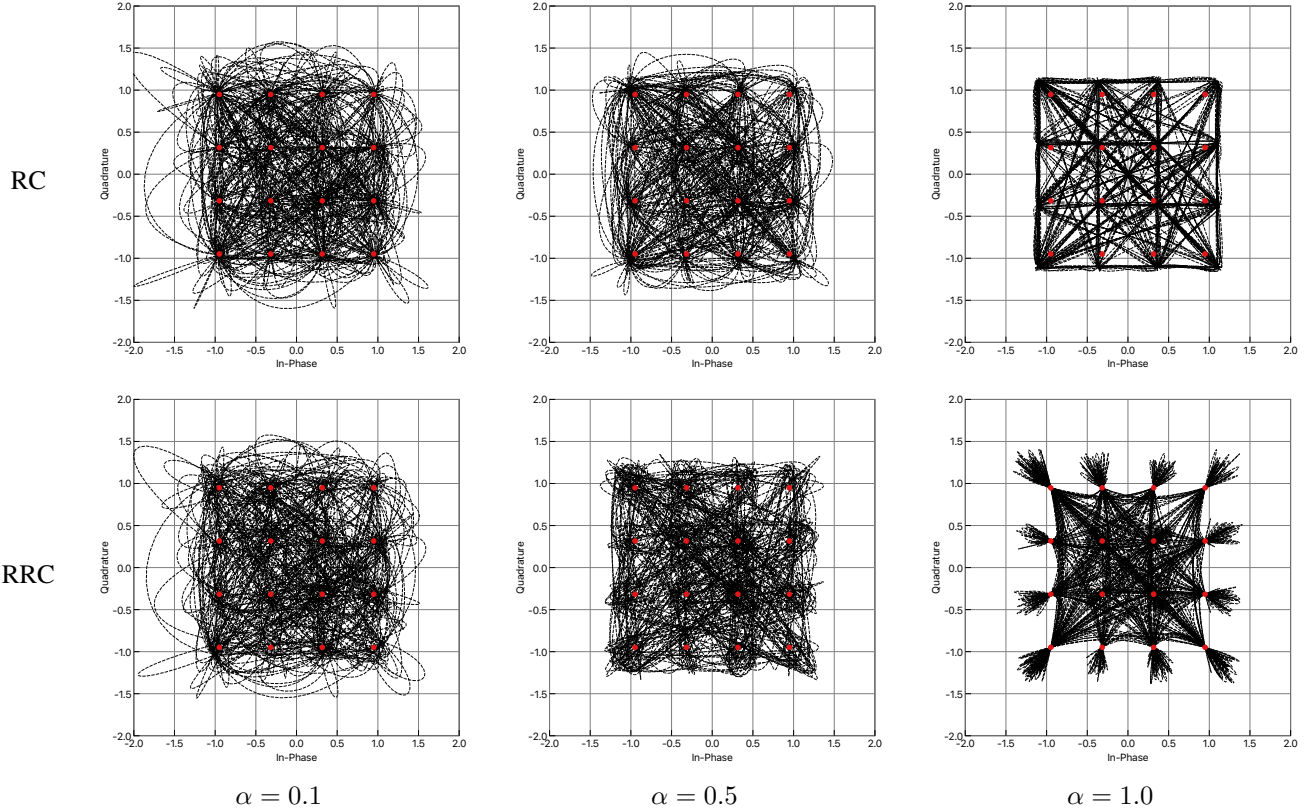


Fig. 3. Example signal trajectories for RC and RRC-filtered 16-QAM signals with various roll-off factors. The red points represent the constellation prior to filtering. The upper and lower figures represent RC and RRC-filtered signals, respectively. The leftmost, middle, and rightmost figures correspond to the roll-off factors of $\alpha = 0.1$, 0.5 , and 1.0 , respectively.

issue is how to determine the effective length of impulse response as it depends on the roll-off factor α . The truncation of energy may lead to OOB spectrum emission as well as ISI, which should be made negligible.

Let us define the energy loss due to the truncation of the impulse response by the rectangular window of range $(-\tau_0, \tau_0)$ as

$$\begin{aligned} L(\tau_0) &\triangleq 1 - \int_{-\tau_0}^{\tau_0} g^2(\tau) d\tau \\ &= 1 - 2 \int_0^{\tau_0} g^2(\tau) d\tau. \end{aligned} \quad (32)$$

In the case of $\alpha = 0$, we may express

$$L(\tau_0) = 1 - \left(\frac{2\text{Si}(2\pi\tau_0)}{\pi} + \frac{\cos(2\pi\tau_0) - 1}{\tau_0\pi^2} \right), \quad (33)$$

where the sine integral is expressed as

$$\text{Si}(x) = \int_0^x \frac{\sin t}{t} dt. \quad (34)$$

In Fig. 2, we demonstrate the relationship between the window size $(-\tau_0, \tau_0)$ and energy loss $L(\tau_0)$ (in decibel scale) for the RC and RRC filters with several representative roll-off factors. These plots are obtained by numerical integration of $g(\tau)$ according to (32), except for the case of $\alpha = 0$ where we apply (33). We observe that as α approaches 0, the filter length τ_0 should be increased substantially so as to maintain the energy loss below a given level. Conversely, if we increase

α even slightly from 0, the required window size significantly decreases. (The case of α as low as 0.03 was reported in [33] for the RRC filter targeting practical satellite communications.)

E. CCDF Property of RC and RRC Filtered QAM Signals

As we have seen, when α increases, the impulse response quickly converges to zero. In return, as observed from Fig. 1, the amplitude of $g(\tau)$ around $\tau = 0$ increases, and this may affect the peak power property. To see this, signal trajectories in the cases of the RC and RRC-filtered 16-QAM signals are compared in Fig. 3. We observe that increasing α reduces signal dynamic range significantly, but when $\alpha = 1$, the signal trajectory exhibits high peak values around the corner points especially in the case of RRC filter, which we refer to as an *overshooting* effect. Therefore, increasing α may not be necessarily desirable from the viewpoint of signal dynamic range.

We now investigate the property of time-averaged CCDF defined by (2) based on simulations. In practice, we may obtain the average by sampling J equidistant signal points (oversampling factor of J compared to the Nyquist rate) as

$$\text{CCDF}(\zeta)_{\text{av}} \approx \frac{1}{J} \sum_{k=0}^{J-1} \text{CCDF} \left(\zeta \mid \frac{k}{J} \right). \quad (35)$$

In Fig. 4, we plot the CCDF of RC and RRC-filtered single-carrier 64-QAM signals evaluated with $J = 16$, as well as that of DFT-precoded OFDM with $N = 512$. The stationary

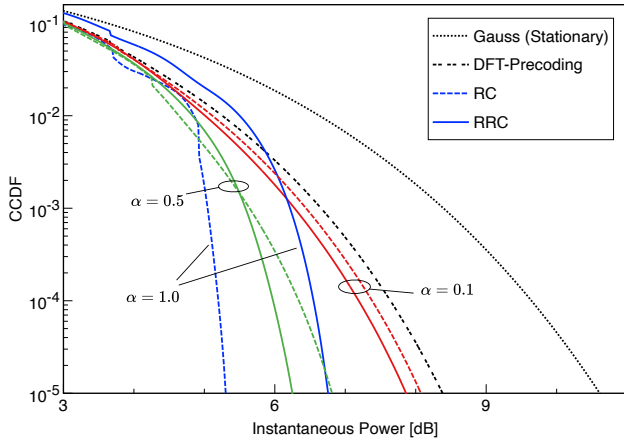


Fig. 4. CCDF of instantaneous power of RC and RRC-filtered 64-QAM signals (simulation) with $J = 16$. For DFT-precoded OFDM, we set $N = 512$.

Gaussian case of (22) is also plotted as an approximation to OFDM signals. We observe that the case of DFT-precoding is worst among the simulated curves, even though it is much better than Gaussian case (i.e., OFDM). This is due to the fact that DFT precoded OFDM corresponds to the single-carrier signal with block transmission, where its impulse response is given by the periodic sinc function as observed from (17). Therefore, it can be seen as an approximation of single-carrier signals with ideal rectangular filtering ($\alpha = 0$).

On the other hand, while increasing α will help reducing the peak power in general, the CCDF in the case of RRC filter with $\alpha = 1$ shows higher value than that with $\alpha = 0.5$ due to the overshooting effect as observed in Fig. 3. Therefore, we clearly see that there should be an optimal value of α in terms of CCDF property for the RRC filter.

We note that an upper bound of the PAPR for the RRC-filtered single-carrier signals is analyzed in [34], and the statistical distributions of its instantaneous power are numerically evaluated in [11, 15].

F. CCDF Property of Filtered Gaussian Signals

From the viewpoint of information theory, the optimal signaling that achieves channel capacity over an AWGN channel is Gaussian. Suppose $\{X_k\}$ in (7) are i.i.d. circularly symmetric complex Gaussian. Then, for any given time instant τ , $s(\tau)$ can be complex Gaussian distributed by the fact that linear combinations of Gaussian random variables are also Gaussian random variables. Therefore, as discussed in [15], $s(\tau)$ is a complex Gaussian random variable with zero mean and variance given by (30). The CCDF is then given by

$$\text{CCDF}(\zeta | \tau) = e^{-\frac{\zeta}{1+b_2 \cos(2\pi\tau)}} \quad (36)$$

and thus its time average is

$$\text{CCDF}(\zeta)_{\text{av}} = \int_0^1 e^{-\frac{\zeta}{1+b_2 \cos(2\pi\tau)}} d\tau \quad (37)$$

which can be easily calculated numerically.

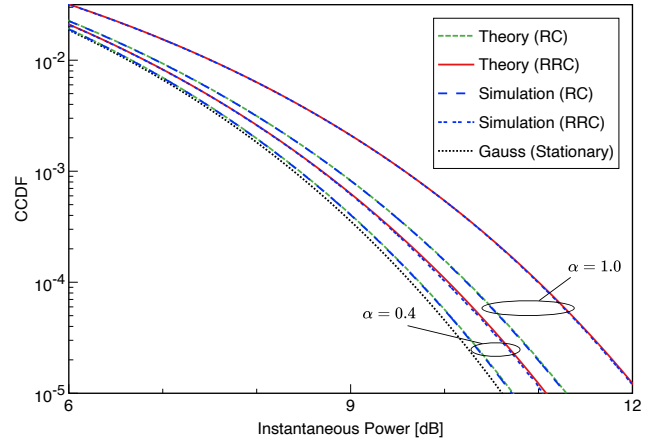


Fig. 5. CCDF of instantaneous power of RC and RRC-filtered Gaussian signals ($\alpha = 0, 0.4$, and 1.0). The result is shown in the range of $\zeta > 2$ where the stationary case ($\alpha = 0$) is optimal.

In Fig. 5, we plot the theoretical as well as simulated CCDF of instantaneous power for the RC and RRC-filtered Gaussian signals with several representative values of roll-off factor α . It is observed that the optimal α that gives the lowest CCDF value is $\alpha = 0$ for the selected range, i.e., $\zeta > 2$ (6 dB). In fact, the following theorem holds for any (including square-root) Nyquist filter of the form (23):

Theorem 1: For $s(\tau)$ of (7) with $\{X_k\}$ given by i.i.d. complex Gaussian with zero mean and unit variance, the time-averaged CCDF is bounded as

$$\text{CCDF}(\zeta)_{\text{av}} \geq e^{-\zeta} \quad \text{for } \zeta > 2 + \varepsilon, \quad (38)$$

with given $\varepsilon \geq 0$, and the equality in (38) holds if and only if the filter is ideal low-pass and in this case $\varepsilon = 0$.

The proof is given in Appendix C.

The above theorem states that in the case of Gaussian signals, the *optimal* filter in terms of CCDF of instantaneous power is the ideal rectangular shape ($\alpha = 0$), where the optimality holds for the region with $\zeta > 2$, i.e., the threshold instantaneous power ζ is above 6 dB, which is often of practical interest. This behavior can be intuitively explained as follows: When the input symbol is Gaussian and $\alpha = 0$, it becomes stationary as discussed in [12], i.e., the distribution of $s(\tau)$ becomes identical for any value of τ . In general cases with $\alpha \neq 0$, on the other hand, it is strictly cyclo-stationary and thus the distribution may vary depending on the value of τ in the range of $[0, 1)$, resulting in higher CCDF values than that of the stationary case when it is averaged over one period.

Remark: Even though the system with $\alpha = 0$ is infeasible in practice, it can be implemented through block transmission as described in Section II-C. Also, if the transmit symbol is close to Gaussian, there would be no benefit of applying DFT-precoding over frequency-selective channels. Therefore, we may conclude that the block transmission through OFDM with channel coding should be a well-motivated practical approach in view of error performance over frequency-selective fading channels, complexity of transmitter/receiver, as well as signal dynamic range, provided that ISI caused by time-selectiveness of channel should be negligible.

IV. HIGH-ORDER MOMENT EXPRESSIONS FOR LINEARLY MODULATED SIGNALS

The previous section has shown that CCDF of instantaneous power of filtered signals varies depending on its roll-off factor as well as signal constellations, but the results can be analyzed only through numerical evaluation, which offers less theoretical insight. In this section, we analyze high-order moments of RC and RRC-filtered signals by developing their closed-form expressions.

As discussed in Section II-A, higher-order moments serve as theoretical benchmarks for their signal dynamic range, i.e., higher values of moments tend to yield higher signal dynamic range, leading to lower efficiency of power amplifiers. Thus, investigating higher-order moments of various filtered signals may offer an insight on their applications to the systems that require high power amplifier efficiency as well as high spectral efficiency. Furthermore, unlike CCDF based analysis, these moments can be efficiently formulated in closed forms if we exploit the cumulants of signal constellation [12]. Thus, we start with a brief review of cumulants, followed by its application to the clipped Gaussian case (as an example of quasi-Gaussian constellations).

A. Review of Cumulants

For a complex random variable $X \in \mathbb{C}$, the even-order cumulants of X (up to the sixth-order) can be derived in terms of its moments as [12, 35]

$$c_2(X) = m_2(X) - |\mu_1(X)|^2, \quad (39)$$

$$c_4(X) = m_4(X) - 2m_2^2(X) - |\mu_2(X)|^2, \quad (40)$$

$$c_6(X) = m_6(X) - 9m_4(X)m_2(X) + 12m_3^2(X) + 18m_2(X)|\mu_2(X)|^2 - 6\Re\{\mu_2(X)\mu_{2,2}^*(X)\} - |\mu_3(X)|^2 - 9|\mu_{2,1}(X)|^2, \quad (41)$$

where [12]

$$m_{2n}(X) \triangleq E\{|X|^{2n}\},$$

$$\mu_{2n,m}(X) \triangleq E\{|X|^{2n}X^m\},$$

$$\mu_m(X) \triangleq E\{X^m\},$$

with n and m representing non-negative integers. For many constellations with symmetry of interest, we have

$$\mu_{2,1}(X) = \mu_{2,2}(X) = \mu_1(X) = \mu_2(X) = \mu_3(X) = 0. \quad (42)$$

Therefore, the cumulants are simplified as

$$c_2(X) = m_2(X), \quad (43)$$

$$c_4(X) = m_4(X) - 2m_2^2(X), \quad (44)$$

$$c_6(X) = m_6(X) - 9m_4(X)m_2(X) + 12m_3^2(X). \quad (45)$$

The cumulants of some representative modulation formats, with its second moment normalized to unity, are listed in Table I. Note that $c_4(X)$ may take a negative value according to the relationship (44), whereas $c_{2n}(X) = 0$ for $n \geq 2$ if X is a circularly symmetric complex Gaussian random variable, i.e., $X \sim \mathcal{CN}(0, 1)$.

TABLE I
CUMULANTS OF REPRESENTATIVE MODULATION FORMATS

| X | QPSK | M^2 -QAM | Gauss |
|----------|------|---|-------|
| $c_2(X)$ | 1 | 1 | 1 |
| $c_4(X)$ | -1 | $-\frac{3}{5}\frac{M^2+1}{M^2-1}$ | 0 |
| $c_6(X)$ | 4 | $\frac{12}{7}\frac{M^4+M^2+1}{(M^2-1)^2}$ | 0 |

B. Cumulants for Clipped Gaussian Case

We investigate a special case of Gaussian signal where its amplitude is controlled to be finite. More specifically, let X denote a complex Gaussian random variable with zero mean and unit variance, i.e., $\mathcal{CN}(0, 1)$. We consider the clipped Gaussian signal, which can be generated as follows:

$$\tilde{X} = \begin{cases} \gamma e^{j \arg X}, & \text{if } |X| > \gamma, \\ X, & \text{otherwise,} \end{cases} \quad (46)$$

where γ corresponds to the clipping ratio [36].

We now derive the cumulant expressions for \tilde{X} . The signal envelope $R \triangleq |X|$ before clipping follows Rayleigh distribution with its probability density function (PDF) given by

$$p_R(r) = 2re^{-r^2}, \quad (47)$$

and that after clipping, i.e., $\tilde{R} \triangleq |\tilde{X}|$, is expressed as

$$p_{\tilde{R}}(r) = 2re^{-r^2}u(\gamma - r) + e^{-\gamma^2}\delta(r - \gamma), \quad (48)$$

where $\delta(x)$ is the Dirac delta function and $u(x)$ is the unit step function with $u(x) = 1$ if and only if $x > 0$ and $u(x) = 0$ otherwise. Using the above expression, we can obtain the following closed-form solution for its high-order moments:

$$m_{2n}(\tilde{X}) = E\{\tilde{R}^{2n}\} = \frac{n!}{(1 - e^{-\gamma^2})^n} \left\{ 1 - e^{-\gamma^2} \sum_{k=0}^{n-1} \frac{1}{k!} \gamma^{2k} \right\}. \quad (49)$$

Note that we may express $\tilde{X} = \tilde{R}e^{j\phi}$, where ϕ is uniformly distributed by assumption. Therefore, from (44) and (45), we have $c_4(\tilde{X})$ and $c_6(\tilde{X})$ as

$$c_4(\tilde{X}) = \frac{2e^{-\gamma^2}}{(1 - e^{-\gamma^2})^2} (1 - \gamma^2 - e^{-\gamma^2}), \quad (50)$$

$$c_6(\tilde{X}) = \frac{3e^{-\gamma^2}}{(1 - e^{-\gamma^2})^3} \times \left\{ (2 - 4\gamma^2 + \gamma^4) - 6e^{-\gamma^2}(1 - \gamma^2) + 4e^{-2\gamma^2} \right\}. \quad (51)$$

If the hard envelope limiter is applied, i.e., $\gamma \rightarrow 0$, it follows that

$$\lim_{\gamma \rightarrow 0} c_4(\tilde{X}) = -1, \quad \lim_{\gamma \rightarrow 0} c_6(\tilde{X}) = 4, \quad (52)$$

which agree with those of QPSK listed in Table I, whereas if no clipping is applied, i.e., in the case of $\gamma \rightarrow \infty$, we have

$$\lim_{\gamma \rightarrow \infty} c_4(\tilde{X}) = 0, \quad \lim_{\gamma \rightarrow \infty} c_6(\tilde{X}) = 0, \quad (53)$$

which agree with those of Gaussian as expected.

Note that the clipped Gaussian signal model with ideal (sinc-function) filtering ($\alpha = 0$) serves as a good approximation for OFDM system with Nyquist-rate clipping, which was investigated in [37].

C. Moment Expressions Using Cumulants

The cumulant has the following important property: If $\{X_k\}$ are mutually independent and $\{\beta_k\}$ are complex-valued constants, we may express

$$c_{2n} \left(\sum_k \beta_k X_k \right) = \sum_k |\beta_k|^{2n} c_{2n}(X_k). \quad (54)$$

The above property indicates that the cumulants for complex random variables are invariant for any constant phase shift.

If the input signals $\{X_k\}$ of $s(\tau)$ in (7) are i.i.d. and meet the condition (42), which are the cases for the standard QAM, circularly symmetric Gaussian, as well as clipped Gaussian [12], then the fourth-order moment of $s(\tau)$ can be expressed, based on the relationships (43)-(45), as [12, Eq.(50)]

$$m_4(s(\tau)) = 2a_2^2(\tau) + a_4(\tau) c_4(X) \quad (55)$$

and its sixth-order moment as [12, Eq.(62)]

$$m_6(s(\tau)) = 6a_2^3(\tau) + 9a_4(\tau) a_2(\tau) c_4(X) + a_6(\tau) c_6(X), \quad (56)$$

where

$$a_{2n}(\tau) \triangleq \sum_{k=-\infty}^{\infty} |g(\tau+k)|^{2n} \quad (57)$$

for a given normalized impulse response $g(\tau)$.

With time averaging, it follows that

$$\overline{m_4} = 2\overline{a_2^2} + \overline{a_4} c_4(X), \quad (58)$$

$$\overline{m_6} = 6\overline{a_2^3} + 9\overline{a_4 a_2} c_4(X) + \overline{a_6} c_6(X), \quad (59)$$

where $\overline{a_n}$, $\overline{a_n^m}$, and $\overline{a_n a_m}$ are the time averaged values of $a_n(\tau)$, $a_n^m(\tau)$, and $a_n(\tau) a_m(\tau)$, respectively, for given positive integers n and m .

In the case of RC and RRC filters, all the coefficients that appear in (58) and (59) can be expressed in closed form and they are summarized in Appendix B.

V. NUMERICAL RESULTS

Given general expressions of high-order moments of linearly modulated signals with i.i.d. input symbols, in this section we numerically evaluate their dependence on the roll-off factors in the case of RC and RRC filters as practical examples.

Based on the above closed-form expressions of the fourth and sixth-order moments developed in the previous section, along with the coefficients derived in Appendix B, we compare them for various modulation formats as a function of roll-off factor α .

A. QAM Cases

The time-averaged fourth and sixth-order moments for QPSK, 16-QAM, 64-QAM, as well as Gaussian constellation are compared in Fig. 6. Those obtained by the corresponding Monte-Carlo simulations are also plotted for several representative cases of α , where they perfectly match with the theoretical values. We clearly observe that the best roll-off factor depends on the modulation format as well as the type of filter, and DFT-precoded OFDM (corresponding to the single-carrier case with $\alpha = 0$) has higher moments than the RC and RRC-filtered single-carrier systems of the same modulation format provided that α is chosen from its practical range (i.e., $\alpha \leq 0.5$).

Furthermore, in the case that the modulated symbol is Gaussian, we observe that the stationary case (i.e., $\alpha = 0$), which corresponds to the conventional OFDM with block transmission, is optimal in view of high-order moments. This observation agrees with the consequence from Theorem 1, which states that the CCDF of the instantaneous power of *filtered* Gaussian signal is minimized if and only if the ideal rectangular filter of $\alpha = 0$ is employed.

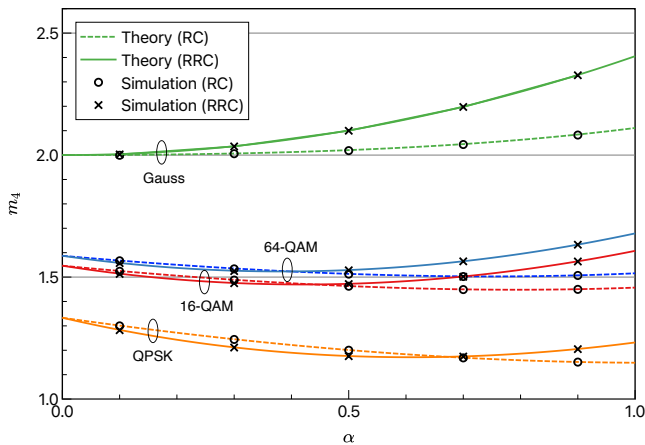
B. Clipped Gaussian Cases

Finally, we compare the time-averaged fourth and sixth-order moments for clipped Gaussian cases with several representative values of clipping ratio γ in Fig. 7. Those based on the corresponding Monte-Carlo simulations are also plotted, where we observe perfect agreement as well. By increasing the parameter γ , the constellation approaches Gaussian. As γ increases, we observe that the optimal value of α approaches zero, which confirms the fact that when the signal approaches Gaussian so as to achieve higher spectral efficiency, it justifies the use of block transmission (i.e., $\alpha = 0$), rather than filtering, from the viewpoint of power amplifier efficiency.

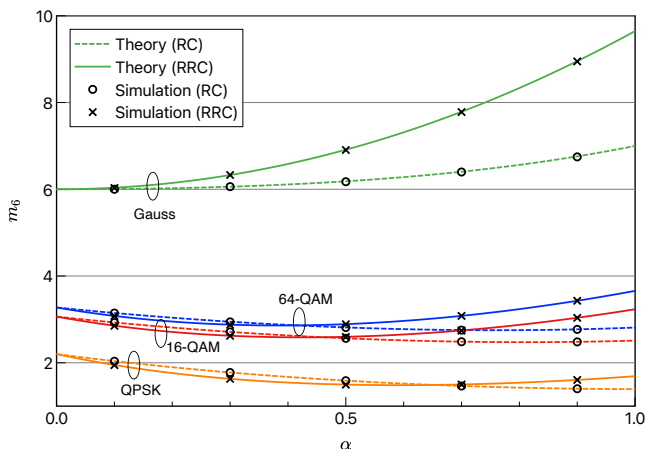
VI. CONCLUSION

We have investigated the statistical behavior of RC and RRC-filtered single-carrier signals with various modulation formats in terms of the fourth and sixth-order moments as a function of spectral efficiency (i.e., the roll-off factor). It has turned out that if the modulated symbol is close to Gaussian, the best approach in view of minimizing signal dynamic range is to employ OFDM-based block transmission schemes since the generated signal becomes stationary and thus time-averaged CCDF of its instantaneous power can be minimized.

The major assumption in this work is that the transmit symbols are i.i.d. such that they can be readily analyzed in terms of high-order moments. In order to efficiently reduce PAPR of transmit signals, common approaches are to make the transmit symbols correlated such that the resulting signal will have lower fluctuation than those without correlation. For example, the clipping of oversampled OFDM signals [36] is one effective approach for PAPR reduction. Other approaches include shaping of the continuous symbols such that they can generate signals with low dynamic range [38, 39]. Theoretical analysis of these correlated signals should be challenging, but worth investigating as we aim at the ultimate wireless



(a)



(b)

Fig. 6. Time-averaged moments for RC and RRC-filtered QAM/Gaussian signals. (a) Fourth order. (b) Sixth order.

communication systems with high spectral efficiency as well as high power amplifier efficiency.

Another possible extension of this work would be the high-order moment analysis of other Nyquist filters of recent interest, such as better-than raised-cosine (BTRC) filters [26].

APPENDIX A DERIVATION OF COEFFICIENTS

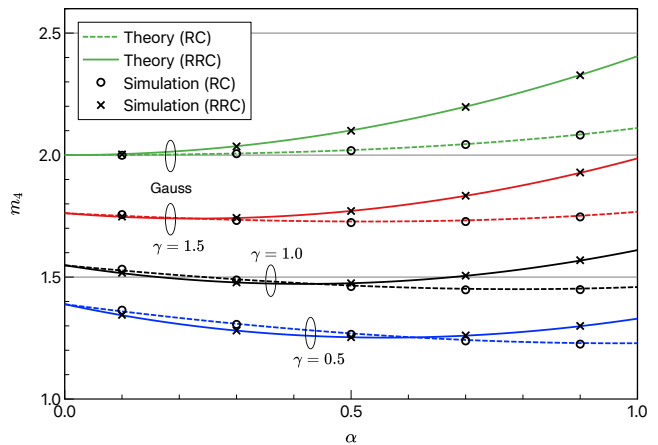
We will derive general expressions of $a_{2n}(\tau)$ expressed by (57) for $n = 1, 2$, and 3 as well as the related coefficients when the frequency response of the filter is given by the form of (23). We then find the specific closed-form expressions for the cases of RC and RRC filters in Appendix B.

In what follows, we denote the time domain function by a lowercase letter, e.g., $z(\tau)$, and its Fourier transform by the corresponding uppercase letter, i.e., $Z(f)$. They are related by

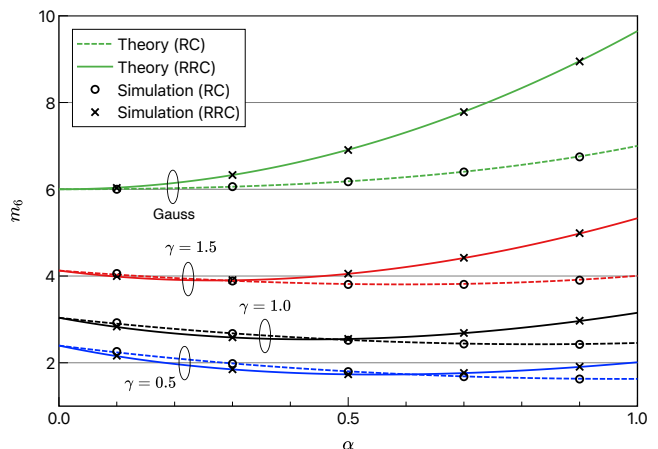
$$Z(f) = \mathcal{F}\{z(\tau)\} \triangleq \int_{-\infty}^{\infty} z(\tau)e^{-j2\pi f\tau} d\tau \quad (\text{A-1})$$

and we write its inverse function as $z(\tau) = \mathcal{F}^{-1}\{Z(f)\}$.

Let $G(f)$ denote a real and even function corresponding to the frequency response under the energy constraint of (25)



(a)



(b)

Fig. 7. Time-averaged moments for RC and RRC-filtered signals with clipped Gaussian input. (a) Fourth order. (b) Sixth order.

with its bandwidth limited to $[-\frac{1+\alpha}{2}, \frac{1+\alpha}{2}]$ for $\alpha \in [0, 1]$ such that

$$G(f) = 0, \quad |f| > \frac{1+\alpha}{2}. \quad (\text{A-2})$$

Let $g(\tau) = \mathcal{F}^{-1}\{G(f)\}$ represent the corresponding impulse response, which is also a real and even function. We may redefine (57) in this case as

$$a_{2n}(\tau) \triangleq \sum_{k=-\infty}^{\infty} g^{2n}(\tau + k), \quad (\text{A-3})$$

and define $\Lambda(f) \triangleq \mathcal{F}\{g^2(\tau)\}$. Since $\Lambda(f) = G(f) \star G(f)$, where \star denotes convolution, it follows that

$$\Lambda(f) = \int_{-\infty}^{\infty} G(\nu)G(\nu - f)d\nu \quad (\text{A-4})$$

with

$$\Lambda(f) = 0, \quad |f| > 1 + \alpha. \quad (\text{A-5})$$

Furthermore, the energy constraint (25) leads to $\Lambda(0) = 1$.

With reference to (A-3), we will derive alternative expressions of $a_{2n}(\tau)$ in terms of $\Lambda(f)$ for $n = 1, 2$, and 3 in what follows.

A. For $n = 1$

The Fourier transform of $a_2(\tau)$ is expressed by a Dirac comb as

$$\begin{aligned} A_2(f) &= \sum_{k=-\infty}^{\infty} H_k(f) \star H_k(f) \\ &= \Lambda(f) \sum_{k=-\infty}^{\infty} e^{j2\pi kf} \\ &= \Lambda(f) \sum_{k=-\infty}^{\infty} \delta(f - k), \end{aligned} \quad (\text{A-6})$$

where $H_k(f) \triangleq G(f)e^{-j2\pi kf}$ is the Fourier transform of $g(\tau - k)$ and $\Lambda(f)$ is expressed by (A-4). Considering the fact that $\Lambda(f)$ is real and symmetric, and also bounded according to (A-5), the inverse Fourier transform of (A-6) is given by

$$\begin{aligned} a_2(\tau) &= \mathcal{F}^{-1}\{A_2(f)\} \\ &= \sum_{k=-\infty}^{\infty} \Lambda(k)e^{j2\pi k\tau} \\ &= \Lambda(0) + 2 \sum_{k=1}^{\infty} \Lambda(k) \cos(2\pi k\tau) \\ &= \overline{a_2} + b_2 \cos(2\pi\tau), \end{aligned} \quad (\text{A-7})$$

where $\overline{a_2} = \Lambda(0) = 1$ corresponds to the time average of $a_2(\tau)$, and the coefficient of the cosine term b_2 can be defined as

$$b_2 \triangleq 2\Lambda(1) = 2 \int_{-\infty}^{\infty} G(f)G(f-1)df. \quad (\text{A-8})$$

Note that $b_2 = 0$ if and only if $G(f)$ does not overlap with $G(f-1)$, i.e., $G(f)$ is the ideal rectangular filter with $\alpha = 0$. As a result, from (A-7), we may express $\overline{a_2^2}$ and $\overline{a_2^3}$ in (58) and (59) as

$$\overline{a_2^2} = \int_0^1 a_2^2(\tau)d\tau = 1 + \frac{1}{2}b_2^2, \quad (\text{A-9})$$

$$\overline{a_2^3} = \int_0^1 a_2^3(\tau)d\tau = 1 + \frac{3}{2}b_2^2. \quad (\text{A-10})$$

B. For $n = 2$

Likewise, the Fourier transform of $a_4(\tau)$ is given by

$$\begin{aligned} A_4(f) &= \sum_{k=-\infty}^{\infty} H_k(f) \star H_k(f) \star H_k(f) \star H_k(f) \\ &= \sum_{k=-\infty}^{\infty} (e^{j2\pi fk} \Lambda(f)) \star (e^{j2\pi fk} \Lambda(f)) \\ &= \sum_{k=-\infty}^{\infty} e^{j2\pi fk} \int_{-\infty}^{\infty} \Lambda(\nu)\Lambda(\nu-f)d\nu \\ &= \sum_{k=-\infty}^{\infty} \delta(f-k) \int_{-\infty}^{\infty} \Lambda(\nu)\Lambda(\nu-f)d\nu. \end{aligned} \quad (\text{A-11})$$

As a result, we have

$$\begin{aligned} a_4(\tau) &= \mathcal{F}^{-1}\{A_4(f)\} \\ &= \sum_{k=-\infty}^{\infty} e^{j2\pi k\tau} \int_{-\infty}^{\infty} \Lambda(\nu)\Lambda(\nu-k)d\nu \\ &= \int_{-\infty}^{\infty} \Lambda(\nu)\Lambda(\nu)d\nu + e^{j2\pi\tau} \int_{-\infty}^{\infty} \Lambda(\nu)\Lambda(\nu-1)d\nu \\ &\quad + e^{-j2\pi\tau} \int_{-\infty}^{\infty} \Lambda(\nu)\Lambda(\nu+1)d\nu \\ &= \overline{a_4} + b_4 \cos(2\pi\tau), \end{aligned} \quad (\text{A-12})$$

where

$$\overline{a_4} \triangleq 2 \int_0^{1+\alpha} \Lambda^2(\nu)d\nu \quad (\text{A-13})$$

corresponds to the time average of $a_4(\tau)$, and

$$b_4 \triangleq 2 \int_{-\alpha}^{1+\alpha} \Lambda(\nu)\Lambda(\nu-1)d\nu \quad (\text{A-14})$$

is the coefficient of the cosine term that will be averaged out.

From (A-7) and (A-12), we may express $\overline{a_4 a_2}$ in (59) as

$$\overline{a_4 a_2} = \int_0^1 a_4(\tau)a_2(\tau)d\tau = \overline{a_4} + \frac{1}{2}b_2 b_4. \quad (\text{A-15})$$

C. For $n = 3$

Similar to the cases with $n = 1$ and $n = 2$, we may express

$$\begin{aligned} A_6(f) &= \sum_{k=-\infty}^{\infty} (e^{j2\pi fk} \Lambda(f)) \star (e^{j2\pi fk} \Lambda(f)) \star (e^{j2\pi fk} \Lambda(f)) \\ &= \sum_{k=-\infty}^{\infty} e^{j2\pi fk} \int_{-\infty}^{\infty} \int_{-\infty}^{\infty} \Lambda(\nu)\Lambda(\nu-\mu)\Lambda(\mu-f)d\nu d\mu \\ &= \sum_{k=-\infty}^{\infty} \delta(f-k) \int_{-\infty}^{\infty} \int_{-\infty}^{\infty} \Lambda(\nu)\Lambda(\nu-\mu)\Lambda(\mu-f)d\nu d\mu. \end{aligned} \quad (\text{A-16})$$

Therefore, we have

$$\begin{aligned} a_6(\tau) &= \mathcal{F}^{-1}\{A_6(f)\} \\ &= \sum_{k=-\infty}^{\infty} e^{j2\pi k\tau} \int_{-\infty}^{\infty} \int_{-\infty}^{\infty} \Lambda(\nu)\Lambda(\nu-\mu)\Lambda(\mu-k)d\nu d\mu \\ &= \int_{-\infty}^{\infty} \int_{-\infty}^{\infty} \Lambda(\nu)\Lambda(\nu-\mu)\Lambda(\mu)d\nu d\mu \\ &\quad + e^{j2\pi\tau} \int_{-\infty}^{\infty} \int_{-\infty}^{\infty} \Lambda(\nu)\Lambda(\nu-\mu)\Lambda(\mu-1)d\nu d\mu \\ &\quad + e^{-j2\pi\tau} \int_{-\infty}^{\infty} \int_{-\infty}^{\infty} \Lambda(\nu)\Lambda(\nu-\mu)\Lambda(\mu+1)d\nu d\mu \\ &= \overline{a_6} + b_6 \cos(2\pi\tau), \end{aligned} \quad (\text{A-17})$$

where

$$\overline{a_6} \triangleq \int_{-(1+\alpha)}^{1+\alpha} \int_{-(1+\alpha)}^{1+\alpha} \Lambda(\mu)\Lambda(\nu)\Lambda(\nu-\mu)d\nu d\mu \quad (\text{A-18})$$

corresponds to the time average of $a_6(\tau)$ and

$$b_6 \triangleq 2 \int_{-(1+\alpha)}^{1+\alpha} \int_{-(1+\alpha)}^{1+\alpha} \Lambda(\mu)\Lambda(\nu)\Lambda(\nu - \mu - 1)d\nu d\mu \quad (\text{A-19})$$

is the coefficient of the cosine term that will be averaged out. Note that the calculation of b_6 in (A-19) is not required as long as one is interested in identifying the time-averaged moments up to the sixth order, which is the case with this work.

APPENDIX B

CLOSED-FORM EXPRESSIONS OF RELATED COEFFICIENTS FOR RC AND RRC FILTERS

In this appendix, we derive closed-form expressions for b_2 , \bar{a}_4 , b_4 , and \bar{a}_6 , in the cases of RC and RRC filters, which are necessary to evaluate (58) and (59). Note that once the above terms are given, \bar{a}_2^2 , \bar{a}_3^2 , and $\bar{a}_4\bar{a}_2$ can be calculated by (A-9), (A-10), and (A-15), respectively. In the subsequent development, to simplify the final equations, we introduce the following notations:

$$\epsilon_0 \triangleq \pi(3\alpha - 1), \quad (\text{B-1})$$

$$\epsilon_1 \triangleq \pi(2\alpha - 1), \quad (\text{B-2})$$

$$\epsilon_2 \triangleq \pi(3\alpha - 2). \quad (\text{B-3})$$

A. Coefficient b_2

Substituting $G(f)$ of (23) into (A-8), and performing integration, we may find b_2 as shown in (31).

B. Coefficient \bar{a}_4

The function $\Lambda(f)$ can be calculated according to (A-4) based on which the term \bar{a}_4 in (A-13) can be obtained. The results are classified by the value of α and expressed as

$$\bar{a}_4 = \begin{cases} B_0, & 0 \leq \alpha < \frac{1}{2}, \\ B_0 + \psi_1, & \frac{1}{2} \leq \alpha \leq 1, \end{cases} \quad (\text{B-4})$$

where the constants B_0 and ψ_1 will have different values depending on the type of filters.

1) RC Filter:

$$B_0 = \frac{128\pi^2 + 192(8 - \pi^2)\alpha^2 - (1359 - 150\pi^2)\alpha^3}{12\pi^2(4 - \alpha)^2}, \quad (\text{B-5})$$

$$\psi_1 = \frac{-1}{6\pi^3(4 - \alpha)^2} \times \left\{ 8\epsilon_1(\epsilon_1^2 - 24\alpha^2) + 9\alpha(2\epsilon_1^2 - 35\alpha^2) \sin\left(\frac{\pi}{\alpha}\right) + \epsilon_1(\epsilon_1^2 - 123\alpha^2) \cos\left(\frac{\pi}{\alpha}\right) \right\}. \quad (\text{B-6})$$

2) RRC Filter:

$$B_0 = \frac{1}{6\pi^3} \left\{ 4\pi^3 - 12(\pi - 4)\pi^2\alpha + 12\pi(40 - 16\pi + \pi^2)\alpha^2 - (1536 + 102\pi - 192\pi^2 + \pi^3)\alpha^3 \right\}, \quad (\text{B-7})$$

$$\psi_1 = \frac{1}{6\pi^3} \left\{ -48\epsilon_1^2\alpha + 1536\alpha^3 + \epsilon_1(\epsilon_1^2 - 348\alpha^2) \sin\left(\frac{\pi}{2\alpha}\right) - 6(5\epsilon_1^2 - 256\alpha^2)\alpha \cos\left(\frac{\pi}{2\alpha}\right) \right\}. \quad (\text{B-8})$$

C. Coefficient b_4

Likewise, from (A-14), we may classify b_4 as

$$b_4 = \begin{cases} C_0, & 0 \leq \alpha < \frac{1}{2}, \\ C_0 + \eta_1, & \frac{1}{2} \leq \alpha \leq 1, \end{cases} \quad (\text{B-9})$$

where the constants C_0 and η_1 will have different values depending on the type of filters.

1) RC Filter:

$$C_0 = \frac{16\pi^2 + 48(\pi^2 - 8)\alpha^2 + (453 - 50\pi^2)\alpha^3}{3\pi^2(\alpha - 4)^2}, \quad (\text{B-10})$$

$$\eta_1 = \frac{7}{24\pi^3(4 - \alpha)^2} \times \left\{ 8\epsilon_1(\epsilon_1^2 - 24\alpha^2) + 9\alpha(2\epsilon_1^2 - 35\alpha^2) \sin\left(\frac{\pi}{\alpha}\right) + \epsilon_1(\epsilon_1^2 - 123\alpha^2) \cos\left(\frac{\pi}{\alpha}\right) \right\}. \quad (\text{B-11})$$

We note that η_1 of (B-11) is related to ψ_1 of (B-6) by $\eta_1 = -\frac{7}{4}\psi_1$.

2) RRC Filter:

$$C_0 = \frac{1}{3\pi^3} \left\{ \pi^3 + 6(4 - \pi)\pi^2\alpha + 12(2 - \pi)^2\pi\alpha^2 + 2(180 - 48\pi + 9\pi^2 - 4\pi^3)\alpha^3 \right\}, \quad (\text{B-12})$$

$$\eta_1 = \frac{1}{24\pi^3} \left\{ 8\epsilon_1(\epsilon_1^2 + 48\alpha^2) + 36\alpha(3\epsilon_1^2 - 70\alpha^2) \sin\left(\frac{\pi}{2\alpha}\right) + \epsilon_1(5\epsilon_1^2 - 876\alpha^2) \cos\left(\frac{\pi}{2\alpha}\right) \right\}. \quad (\text{B-13})$$

D. Coefficient \bar{a}_6

Finally, we obtain \bar{a}_6 from (A-18) as

$$\bar{a}_6 = \begin{cases} D_0, & 0 \leq \alpha < \frac{1}{3}, \\ D_0 + \delta_1, & \frac{1}{3} \leq \alpha < \frac{1}{2}, \\ D_0 + \delta_1 + \delta_2, & \frac{1}{2} \leq \alpha < \frac{2}{3}, \\ D_0 + \delta_1 + \delta_2 + \delta_3, & \frac{2}{3} \leq \alpha \leq 1, \end{cases} \quad (\text{B-14})$$

where the constants D_0 , δ_1 , δ_2 , and δ_3 will have different values depending on the type of filters.

1) RC Filter:

$$D_0 = \frac{1}{160\pi^4(4-\alpha)^3} \{5632\pi^4 - 7680\pi^2(\pi^2 - 8)\alpha^2 + 15360(84 - 18\pi^2 + \pi^4)\alpha^4 - 5(348705 - 58485\pi^2 + 2389\pi^4)\alpha^5\}, \quad (\text{B-15})$$

$$\delta_1 = \frac{1}{128\pi^5(4-\alpha)^3} \{32\epsilon_0(\epsilon_0^4 - 120\epsilon_0^2\alpha^2 + 2520\alpha^4) - 45\alpha(\epsilon_0^4 - 210\epsilon_0^2\alpha^2 + 3003\alpha^4)\sin\left(\frac{\pi}{\alpha}\right) - \epsilon_0(\epsilon_0^4 - 885\epsilon_0^2\alpha^2 + 54495\alpha^4)\cos\left(\frac{\pi}{\alpha}\right)\}, \quad (\text{B-16})$$

$$\delta_2 = \frac{3}{64\pi^5(4-\alpha)^3} \{32\epsilon_1(\epsilon_1^4 - 120\epsilon_1^2\alpha^2 + 2520\alpha^4) + 45\alpha(\epsilon_1^4 - 210\epsilon_1^2\alpha^2 + 3003\alpha^4)\sin\left(\frac{\pi}{\alpha}\right) + \epsilon_1(\epsilon_1^4 - 885\epsilon_1^2\alpha^2 + 54495\alpha^4)\cos\left(\frac{\pi}{\alpha}\right)\}, \quad (\text{B-17})$$

$$\delta_3 = \frac{-1}{320\pi^5(4-\alpha)^3} \{32\epsilon_2(\epsilon_2^4 - 120\epsilon_2^2\alpha^2 + 2520\alpha^4) - 45\alpha(\epsilon_2^4 - 210\epsilon_2^2\alpha^2 + 3003\alpha^4)\sin\left(\frac{2\pi}{\alpha}\right) - \epsilon_2(\epsilon_2^4 - 885\epsilon_2^2\alpha^2 + 54495\alpha^4)\cos\left(\frac{2\pi}{\alpha}\right)\}. \quad (\text{B-18})$$

2) RRC Filter:

$$D_0 = \frac{11}{20} + \left(\frac{11}{\pi} - \frac{11}{4}\right)\alpha + \left(\frac{11}{2} + \frac{124}{\pi^2} - \frac{56}{\pi}\right)\alpha^2 - \left(\frac{11}{2} - \frac{768}{\pi^3} + \frac{492}{\pi^2} - \frac{96}{\pi}\right)\alpha^3 + \left(\frac{11}{4} + \frac{6336}{\pi^4} - \frac{4224}{\pi^3} + \frac{852}{\pi^2} - \frac{56}{\pi}\right)\alpha^4 - \left(\frac{33}{160} + \frac{55296}{\pi^5} - \frac{14823}{2\pi^4} - \frac{5088}{\pi^3} + \frac{4707}{8\pi^2} - \frac{1}{\pi}\right)\alpha^5, \quad (\text{B-19})$$

$$\delta_1 = \frac{20\epsilon_0}{\pi^5}(\epsilon_0^2 - 144\alpha^2)\alpha^2 + \frac{\epsilon_0}{\pi^5}\left(\frac{1}{128}\epsilon_0^4 - \frac{545}{32}\epsilon_0^2\alpha^2 + \frac{22005}{8}\alpha^4\right)\sin\left(\frac{\pi}{2\alpha}\right) - \frac{\alpha}{\pi^5}\left(\frac{35}{64}\epsilon_0^4 - \frac{585}{2}\epsilon_0^2\alpha^2 + \frac{45045}{4}\alpha^4\right)\cos\left(\frac{\pi}{2\alpha}\right), \quad (\text{B-20})$$

$$\delta_2 = \frac{5\alpha}{\pi^5}(\epsilon_1^4 - 384\epsilon_1^2\alpha^2 + 12672\alpha^4) - \frac{\epsilon_1}{\pi^5}\left(\frac{3}{64}\epsilon_1^4 - \frac{1515}{16}\epsilon_1^2\alpha^2 + \frac{60885}{4}\alpha^4\right)\sin\left(\frac{\pi}{2\alpha}\right) + \frac{\alpha}{\pi^5}\left(\frac{25}{8}\epsilon_1^4 - \frac{12885}{8}\epsilon_1^2\alpha^2 + 63360\alpha^4\right)\cos\left(\frac{\pi}{2\alpha}\right), \quad (\text{B-21})$$

$$\delta_3 = \frac{\alpha}{\pi^5}(-\epsilon_2^4 + 288\epsilon_2^2\alpha^2 - 8064\alpha^4) + \frac{\alpha}{\pi^5}\left(-\frac{1}{4}\epsilon_2^4 + \frac{1359}{8}\epsilon_2^2\alpha^2 - 8064\alpha^4\right)\sin\left(\frac{\pi}{\alpha}\right) - \frac{\epsilon_2}{\pi^5}\left(\frac{1}{320}\epsilon_2^4 - \frac{141}{16}\epsilon_2^2\alpha^2 + \frac{7119}{4}\alpha^4\right)\cos\left(\frac{\pi}{\alpha}\right). \quad (\text{B-22})$$

APPENDIX C

PROOF OF THEOREM 1

Proof: The time-averaged CCDF of (37) can be expressed as

$$\text{CCDF}(\zeta)_{\text{av}} = E_\tau \left\{ e^{-\frac{\zeta}{1+b_2\cos(2\pi\tau)}} \right\}, \quad (\text{C-1})$$

where τ is a uniform random variable distributed over $[0, 1)$ and the notation $E_x\{\cdot\}$ explicitly indicates that the expectation is taken over x . By changing the random variable as $u = \cos(2\pi\tau)$, we have

$$\text{CCDF}(\zeta)_{\text{av}} = E_u \left\{ e^{-\frac{\zeta}{1+b_2u}} \right\}. \quad (\text{C-2})$$

Let us define the function $f(u)$ as

$$f(u) \triangleq e^{-\frac{\zeta}{1+b_2u}}. \quad (\text{C-3})$$

By differentiating $f(u)$ with respect to u twice, we have

$$f''(u) = \frac{b_2^2 e^{-\frac{\zeta}{1+b_2u}} \zeta \{\zeta - 2(1+b_2u)\}}{(1+b_2u)^4}. \quad (\text{C-4})$$

Therefore, if $\zeta > 2 + 2b_2u$, $f(u)$ is a convex function, and otherwise it is concave. Since $u \leq 1$, $f(u)$ is always convex in the region of $\zeta > 2 + 2b_2$. Therefore, by Jensen's inequality we have

$$\text{CCDF}(\zeta)_{\text{av}} = E_u \{f(u)\} \quad (\text{C-5})$$

$$\geq f(E_u \{u\}) \quad (\text{C-6})$$

$$= e^{-\zeta} \quad (\text{C-7})$$

for $\zeta > 2 + 2b_2$, since $E_u\{u\} = 0$. Note that the equality in (C-6) holds if and only if $b_2 = 0$, in which case $f(u)$ does not depend on u . Consequently, the CCDF value in the region of $\zeta > 2 + 2b_2$ is minimized if and only if $b_2 = 0$. Since $b_2 = 0$ is equivalent to $\alpha = 0$ as shown in Appendix A, Theorem 1 follows with $\varepsilon \triangleq 2b_2$. ■

REFERENCES

- [1] H. Ochiai, "An analysis of band-limited communication systems from amplifier efficiency and distortion perspective," *IEEE Trans. Commun.*, vol. 61, no. 4, pp. 1460–1472, Apr. 2013.
- [2] H. Ochiai and H. Imai, "On the distribution of the peak-to-average power ratio in OFDM signals," *IEEE Trans. Commun.*, vol. 49, no. 2, pp. 282–289, Feb. 2001.
- [3] H. G. Myung, J. Lim, and D. J. Goodman, "Single carrier FDMA for uplink wireless transmission," *IEEE Veh. Technol. Mag.*, vol. 1, no. 3, pp. 30–38, 2006.
- [4] N. Michailow, M. Matthé, I. S. Gaspar, A. N. Caldevilla, L. L. Mendes, A. Festag, and G. Fettweis, "Generalized frequency division multiplexing for 5th generation cellular networks," *IEEE Trans. Commun.*, vol. 62, no. 9, pp. 3045–3061, 2014.
- [5] R. Hadani, S. Rakib, M. Tsatsanis, A. Monk, A. J. Goldsmith, A. F. Molisch, and R. Calderbank, "Orthogonal time frequency space modulation," in *2017 IEEE Wireless Commun. Netw. Conf. (WCNC)*, 2017, pp. 1–6.
- [6] K. Liu, W. Deng, and Y. Liu, "Theoretical analysis of the peak-to-average power ratio and optimal pulse shaping filter design for GFDM systems," *IEEE Trans. Signal Process.*, vol. 67, no. 13, pp. 3455–3470, Jul. 2019.
- [7] G. D. Surabhi, R. M. Augustine, and A. Chockalingam, "Peak-to-average power ratio of OTFS modulation," *IEEE Commun. Lett.*, vol. 23, no. 6, pp. 999–1002, Jun. 2019.
- [8] P. Wei, Y. Xiao, W. Feng, N. Ge, and M. Xiao, "Charactering the peak-to-average power ratio of OTFS signals: A large system analysis," *IEEE Trans. Wireless Commun.*, vol. 21, no. 6, pp. 3705–3720, Jun. 2022.

- [9] E. Bala, J. Li, and R. Yang, "Shaping spectral leakage: A novel low-complexity transceiver architecture for cognitive radio," *IEEE Veh. Technol. Mag.*, vol. 8, no. 3, pp. 38–46, 2013.
- [10] H. Ochiai, "On spectral efficiency of OFDM signals based on windowing," *IEICE Trans. Fundamentals.*, vol. E106-A, no. 5, pp. 752–764, 2023. [Online]. Available: https://www.jstage.jst.go.jp/article/transfun/E106.A/5/E106.A_2022WB10002/_pdf/-char/en
- [11] —, "Exact and approximate distributions of instantaneous power for pulse-shaped single-carrier signals," *IEEE Trans. Wireless Commun.*, vol. 10, no. 2, pp. 682–692, Feb. 2011.
- [12] —, "High-order moments and Gaussianity of single-carrier and OFDM signals," *IEEE Trans. Commun.*, vol. 63, no. 12, pp. 4964–4976, Dec. 2015.
- [13] Y. Saito, Y. Kishiyama, A. Benjebbour, T. Nakamura, A. Li, and K. Higuchi, "Non-orthogonal multiple access (NOMA) for cellular future radio access," in *Proc. 2013 IEEE 77th Vehicular Technology Conference (VTC-Spring)*, 2013, pp. 1–5.
- [14] Z. Ding, X. Lei, G. K. Karagiannidis, R. Schober, J. Yuan, and V. K. Bhargava, "A survey on non-orthogonal multiple access for 5G networks: Research challenges and future trends," *IEEE J. Select. Areas Commun.*, vol. 35, no. 10, pp. 2181–2195, 2017.
- [15] S. Stern and R. F. H. Fischer, "Efficient assessment of the instantaneous power distributions of pulse-shaped single- and multi-carrier signals," in *Proc. First Int. Black Sea Conf. Commun. Netw. (BlackSeaCom)*, 2013, pp. 12–17.
- [16] H. Ochiai, "Fourth-order moment analysis of filtered single-carrier and OFDM signals," in *Proc. 2017 IEEE 86th Veh. Technol. Conf. (VTC-Fall)*, 2017, pp. 1–5.
- [17] D. Falconer, "Linear precoding of OFDMA signals to minimize their instantaneous power variance," *IEEE Trans. Commun.*, vol. 59, no. 4, pp. 1154–1162, 2011.
- [18] C. H. G. Yuen and B. Farhang-Boroujeny, "Analysis of the optimum precoder in SC-FDMA," *IEEE Trans. Wireless Commun.*, vol. 11, no. 11, pp. 4096–4107, Jan. 2012.
- [19] 3GPP Technical Specification Group Radio Access Network WG 1 LTE Adhoc, *Cubic Metric in 3GPP-LTE*. R1-060023, Jan. 2006.
- [20] R. Y. Kim, Y. Y. Kim, A. A. Yazdi, S. Sorour, and S. Valaee, "Joint reduction of peak-to-average power ratio, cubic metric, and block error rate in OFDM systems using network coding," *IEEE Trans. Veh. Technol.*, vol. 60, no. 9, pp. 4363–4373, Nov. 2011.
- [21] K.-H. Kim, J.-S. No, and D.-J. Shin, "On the properties of cubic metric for OFDM signals," *IEEE Signal Process. Lett.*, vol. 23, no. 1, pp. 80–83, Jan. 2016.
- [22] R. K. Mallik and R. Murch, "New exact higher order moment expressions for the PAPR of complex Gaussian variables," *IEEE Wireless Commun. Lett.*, pp. 382–386, Feb. 2024.
- [23] H. Ochiai and H. Imai, "Performance of block codes with peak power reduction for indoor multicarrier systems," in *Proc. 48th IEEE Veh. Technol. Conf. (VTC'98)*, vol. 1, 1998, pp. 338–342.
- [24] H. Ochiai, "On instantaneous power distributions of single-carrier FDMA signals," *IEEE Wireless Commun. Lett.*, vol. 1, no. 2, pp. 73–76, Apr. 2012.
- [25] —, "Statistical distributions of instantaneous power and peak-to-average power ratio for single-carrier FDMA systems," *Phys. Commun.*, vol. 8, pp. 47–55, Sep. 2013.
- [26] N. Beaulieu, C. C. Tan, and M. O. Damen, "A "better than" Nyquist pulse," *IEEE Commun. Lett.*, vol. 5, no. 9, pp. 367–368, Sep. 2001.
- [27] A. Assalini and A. M. Tonello, "Improved Nyquist pulses," *IEEE Commun. Lett.*, vol. 8, no. 2, pp. 87–89, Feb. 2004.
- [28] M. I. M. T. Moazzeni, S. A. Al Hasani and S. J. Hussaini, "On the effect of compactness of pulse shaping function on inter-symbol interference," *IEEE Commun. Lett.*, vol. 26, no. 4, pp. 828–832, Apr. 2022.
- [29] J. G. Proakis and M. Salehi, *Digital Communications*, 5th ed. Boston: McGraw-Hill, 2008.
- [30] Y. Jaffal and A. Alvarado, "Pulses with minimum residual intersymbol interference for faster than Nyquist signaling," *IEEE Commun. Lett.*, vol. 26, no. 11, pp. 2670–2674, Nov. 2022.
- [31] F. A. Aoudia and J. Hoydis, "Waveform learning for next-generation wireless communication systems," *IEEE Trans. Commun.*, vol. 70, no. 6, pp. 3804–3817, Jun. 2022.
- [32] S. Chennakeshu and G. J. Saulnier, "Differential detection of $\pi/4$ -shifted-DQPSK for digital cellular radio," *IEEE Trans. Veh. Technol.*, vol. 42, no. 1, pp. 46–57, Feb. 1993.
- [33] Y. Suzuki, K. Tsuchida, and Y. Matsusaki, "Performance evaluation of transmission system for 8K Super Hi-Vision satellite broadcasting," in *Proc. IEEE GLOBECOM 2014*, 2014, pp. 2886–2891.
- [34] S. Daumont, B. Rihawi, and Y. Louët, "Root-raised cosine filter influences on PAPR distribution of single carrier signals," in *Proc. Int. Symp. Commun., Contr. and Signal Process. (ISCCSP 2008)*, 2008, pp. 841–845.
- [35] V. P. Leonov and A. N. Shiryayev, "On a method of calculation of semi-invariants," *Theory of Probability & its Applications*, vol. 4, no. 3, pp. 319–329, 1959.
- [36] H. Ochiai and H. Imai, "Performance analysis of deliberately clipped OFDM signals," *IEEE Trans. Commun.*, vol. 50, no. 1, pp. 89–101, Jan. 2002.
- [37] —, "Performance of the deliberate clipping with adaptive symbol selection for strictly band-limited OFDM systems," *IEEE J. Select. Areas Commun.*, vol. 18, no. 11, pp. 2270–2277, Nov. 2000.
- [38] H. Ochiai, "A novel trellis shaping design with both peak and average power reduction for OFDM systems," *IEEE Trans. Commun.*, vol. 52, no. 11, pp. 1916–1926, Nov. 2004.
- [39] M. Tanahashi and H. Ochiai, "Near constant envelope trellis shaping for PSK signaling," *IEEE Trans. Commun.*, vol. 57, no. 2, pp. 450–458, Feb. 2009.